Growth of tumor due to Arsenic and its mitigation by black tea in Swiss albino mice

H. M. Srivastava, Urmimala Dey, Archismaan Ghosh, Jai Prakash Tripathi, Syed Abbas, A. Taraphder, & Madhumita Roy

July 2020

Alexandria Engineering Journal (2020) 59, 1345–1357

HOSTED BY

Alexandria University

Alexandria Engineering Journal

www.elsevier.com/locate/aej
www.sciencedirect.com

ORIGINAL ARTICLE

Growth of tumor due to Arsenic and its mitigation by black tea in Swiss albino mice

H.M. Srivastava [a,b,h], Urmimala Dey [c], Archismaan Ghosh [d], Jai Prakash Tripathi [e], Syed Abbas [f,*], A. Taraphder [g,c,f], Madhumita Roy [d]

[a] Department of Mathematics and Statistics, University of Victoria, Victoria, British Columbia V8W 3R4, Canada
[b] Department of Medical Research, China Medical University Hospital, China Medical University, Taichung 40402, Taiwan, Republic of China
[c] Centre for Theoretical Studies, Indian Institute of Technology Kharagpur, Kharagpur 721302, India
[d] Department of Environmental Carcinogenesis and Toxicology, Chittaranjan National Cancer Institute, 37 S. P. Mukherjee Road, Kolkata 700026, India
[e] Department of Mathematics, Central University of Rajasthan, Bandersindri, Kishangarh, Ajmer, 305817 Rajasthan, India
[f] School of Basic Sciences, Indian Institute of Technology, Mandi 175005, India
[g] Department of Physics, Indian Institute of Technology Kharagpur, Kharagpur 721302, India
[h] Department of Mathematics and Informatics, Azerbaijan University, AZ1007 Baku, Azerbaijan

Received 15 January 2020; revised 28 February 2020; accepted 2 March 2020
Available online 20 March 2020

KEYWORDS

Tumor growth dynamics;
Immune response;
Stability theory

Abstract Inorganic arsenic causes carcinogenesis in a large part of the world. Its potential is elicited by the generation of ROS, which leads to damages to DNA, lipid and protein. Black tea, an antioxidant, can mitigate such deleterious effects by quenching ROS. We study Arsenic-toxicity and its amelioration by black tea in a colony of albino mice: a homology exists between the protein coding regions of mice and human. We observe that black tea has salutary effects on tumor-growth: it arrests damaged cell growth and produces early saturation of the damage. The experimental data obtained by us are modelled with dynamical equations. This is followed by a search for steady states and their stability analysis.

1. Introduction

Arsenic, plentifully available in earth's crust [12] is a metalloid, found in both organic and inorganic forms with two oxidation states, +3 (arsenite) and +5 (arsenate). It leaches into the ground water from copper or lead containing rocks. Anthropogenic activities like mining also release it to ground water [14]. Exposure to arsenic happens primarily from drinking water, air and food [4]. A lot of health hazards are indeed correlated to chronic inorganic arsenic (iAs) exposure and the current estimate is about 200 million people in 40 countries have been exposed to high degree of iAs (much higher than permissible limit, 10 μg/l [16]) from ground water alone. Arsenic

* Corresponding author.
E-mail addresses: abbas@iitmandi.ac.in, sabbas.iitk@gmail.com (S. Abbas).
Peer review under responsibility of Faculty of Engineering, Alexandria University.

https://doi.org/10.1016/j.aej.2020.03.001

levels are very high, 50–3200 mg/l in ground water, at several places in India [4].

Inorganic As is a well-known cause of several diseases, cancer included. Excessive ROS generation by iAs is considered the main reason behind disturbed homeostasis of individuals [24]. ROS damages the DNA, lipid and protein. It can also modulate expression of genes [23] implicated in cancer. Regular iAs exposure is known to decrease the activities of antioxidant enzymes, that are required to mitigate the free radicals, due to the generation of ROS [24].

To check the damaging effects of iAs, it is desirable to halt carcinogenesis at the initial stage. Carcinogenesis involves multiple stages: initiation, promotion, progression and finally metastasis. Chemoprevention, is the use of natural, biological or synthetic agents to suppress, reverse or prevent the progression of cancer [29]. To mitigate the effects of iAs-induced toxicity, chemopreventive strategies with natural compounds are preferable. Tea is a good antioxidant and has anticancer properties [25]. It is also the most preferred beverage. As an antioxidant agent, black tea could counter the deleterious effects of ROS generated by arsenic. Studies have been initiated in Swiss Albino mice [26,27] to unravel the preventive role of black tea against iAs-induced carcinogenesis, Black tea quenches the generation of ROS effectively, lipid peroxidation and diminish DNA damage, eliciting its anti-cancer potential.

In this work, we have studied a colony of Swiss albino mice by subjecting them to iAs and a mitigating agent, the black tea. The experimental data thus obtained over a long period was then used to develop a mathematical model which is analyzed thoroughly. The analysis leads us to develop useful conclusions on the effects of iAs and black tea, and the inherent competition therein. The novelty of our approach lies in the nature of the study: a careful, long and detailed experiment is backed by a mathematical analysis. It is shown that such a combined experiment-theory project is necessary not only to model the data, it extends the realm of possibilities beyond the limits of experiment. For example, we were able to incorporate and account for other factors like imunogenesis. In the following we first describe the experiment and then use the data to set up the model analysis. We draw conclusions at the end.

2. Materials and methods

2.1. Chemicals

Tea Extract Preparation1.25 gm of Assam tea was mixed with equal amount of Darjeeling tea. The mixture was brewed in 100 ml of boiled water for 5 min. It was then stored, following lyophilization by a SCANVAC lyophilizer. Prior to administering by gavage to the mice, we weighed and reconstituted the lyophilized powder in water. Catechin and theaflavin contents (both black and green) were then analyzed by HPLC. Following our previous studies and using the epidemiological evidences [24], we ascertained the dose and accordingly, 100 μl of tea-extract was given to the mice.

2.2. Animal maintenance

From our animal house, an inbred colony (IAEC 1774/MR-3/2017/9) 4–5 week old normal, male, Swiss albino mice (Mus Musculus) was selected. These were fed on synthetic pellets for mice-feed. During our study, the mice had access to ad libitum water. Standard conditions with alternate 12 h light and darkness and a temperature of 22 ± 2 ° C were maintained. The mice were finally sacrificed by euthanasia with an overdose of thiopentone sodium.

2.3. Treatment

We divided the colony into four groups, namely I, II, III and IV: Group I: The Control group of mice: fed normal food and tap water. Group II: This group was fed with black tea by gavage. Group III: Supplied with arsenic water for 360 days at the rate of 500 μg/l. Group IV: Black tea (100 mg/ml, thrice daily) and arsenic water (500 μg/ml) both were administered by gavage for the same period. We collected and stored the blood and tissue samples properly for experiments on sacrificing the mice at different times. Two sets of data were generated to determine the damaged cells as time progresses: first dataset with only iAs (for about 360 days) and the second with both iAs and black tea. For this, the data for 330 days were available. Group II showed no toxicity from black tea and so we do not present any data. Some cell damages were already present in the mice at the outset, and the damage cell count therefore starts from a finite value. Fig. 1 shows both the data. The application of black tea clearly brings down the damaged cell count and the damage shows early saturation.

2.4. Estimation of ROS generation

Following Balasubramanyam et al. [3], with slight modifications, the amount of generated reactive Oxygen species in the blood was determined. Solution A (NH_4Cl dissolved in TRIS at pH 7.2) and Solution B (meso-inositol) were used to isolate leukocytes from mice blood and suspended in HBS (Hepes Buffered Saline pH 7.4). After adding 10 mM 2′,7′ dichlorodihydro-fluorescein (DCFH-DA), we incubated it for 45 min in the dark and the fluorescent intensity at 530 nm of the DCF was then duly recorded.

2.5. Single cell gel electrophoresis

Comet assay [28] or Single Cell Gel Electrophoresis (SCGE) was used to estimate the DNA damage from leukocytes isolated from blood. 20 μl of leukocytes were suspended in 0.6% low melting agarose (LMA). These were layered over frosted slide pre-coated with 0.75% normal melting agarose (NMA). Immersing the cells overnight at a temperature of 4° C in lysis buffer (2.5 M NaCl, 0.1 M Na_2EDTA, 10 mM TRIS, 0.3 M NaOH, 10%DMSO and 1% TritonX; pH 10), the cells were put to lysis. We then pre-soaked the slides for 20 min in electrophoresis buffer (10 mM NaOH, 0.2 m Na_2-EDTA; pH>13), which were, for 25 min at 15 V, 220 mA, subjected to electrophoresis subsequently. The slides were viewed under a fluorescence microscope after staining with ethidium bromide.

2.6. Lipid peroxidation assay

With slight modifications of the principle of Okhawa et al. [22] and using lipid peroxidation assay, the cell membrane damage

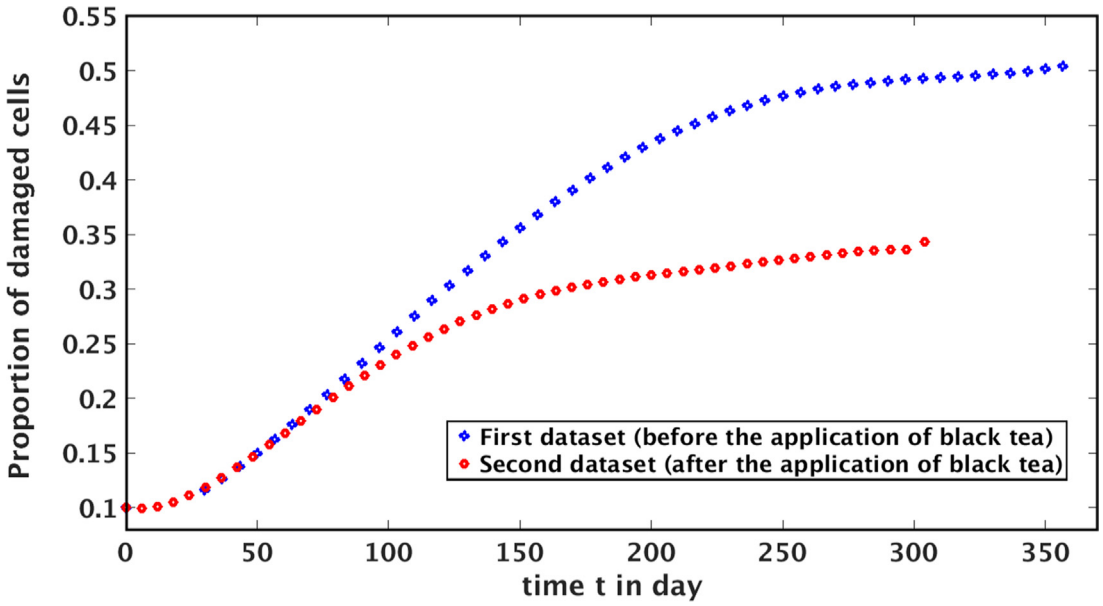

Fig. 1 (upper curve) The cell-damage proportion by iAs. The lower curve is data from the group receiving iAs and black tea both. The amelioration – limiting the extent of damage due to tea, is evident. There is also an early saturation.

due to ROS was estimated. Liver tissues were collected from the sacrificed animals and homogenized. We added 10% SDS, 20% acetic acid and 0.8% TBA to this homogenate after that. It was placed in boiling water for 1 h and transferred straight to ice for 10 min. The samples were subjected to a centrifuge (@2500 rpm, 10 min) then. On collecting the supernatant, we measured absorbance at 535 nm. The lipid peroxidation was found out as the number of moles of Malondialdehyde (MDA) generated.

3. A model for cell damage growth

We model the effects of iAs and black tea on the observed growth of damaged cells in the colony of Swiss albino mice by a set of simple mathematical equations. We have two sets of data from the experiment for the growth of damaged cells, one with iAs only (at 500 μg/l) and the other with As and tea (100 mg/ml, thrice daily). The black tea is the mitigating agent. The ROS generated gives a measure of the extent of cell damage. The effect of immunity is ignored to start with and we understand what iAs and tea do to the cell damage. The immune cell response will be brought on later. In this and the following section, we try to model our experimental data using standard mathematical models, in line with previous studies on the mathematical models of growth of tumor cells [15,6,5]. There exist comprehensive articles on such models and their merits (see, Altrock, et al. [1] and Pillis, *et al.*, [7]). For more works in the field of mathematical modelling, we refer to reader [10,18,19,17,2]. There is no need, therefore, to digress on details of such models here.

The growth of damaged cells is represented by the well known growth model:

$$\frac{dn}{dt} = rn(1 - \frac{n}{K}) \tag{1}$$

ROS data give an estimate of N in the above equation, a measure of the damaged cells. Here $n = \frac{N}{N_0}$, with N_0 being the total number of cells at $t = 0$. Note that the actual values of either N or N_0 are irrelevant, only the percentage of damaged cells n, is needed. The model has two unknown constants, r and $K = B/N_0$, where B provides the well-known 'carrying capacity'. The iAs was administered daily from outside at a fixed rate. It is represented by the term αAn in the model while the mitigating effects of tea are taken in by βTn term [21]. The overall model for the cell growth then is

$$\frac{dn}{dt} = rn(1 - \frac{n}{K}) + \alpha An - \beta Tn \tag{2}$$

α and β are unknown constants, fitted from our data. The equations for the concentration of iAs and tea, (quantities A and T respectively), are similar [21]. In principle, there ought to be additional processes; in the minimal model however, we consider the intake of iAs and tea by standard decay terms with sources:

$$\frac{dA}{dt} = A_0 - \gamma_A A \tag{3}$$

$$\frac{dT}{dt} = T_0 - \gamma_T T \tag{4}$$

In these equations A_0 and T_0 are the external source terms of iAs and tea. Other effects of iAs and tea on the body could be there and should be considered, which we will in the future. One effect, usually considered important, but we neglect here (see next section), is the immune-surveillance. A_0 and T_0, the so-called dosage, are reported in mg (or ml)/day. However, to incorporate them in the Eq. (2), one needs their concentrations at the cellular level. These data are not available to us from the experiment at hand. We leave them to the fitting. Note that for the case with only iAs administered (no tea), the equation for tea is redundant.

We need to account for the expulsion of iAs and tea from the body via usual decay rates (very rough estimates of half-lives of for these are available), γ_A and γ_T. Note that different ingredients decay differently, depend also on the organ in question. Some approximate values are available in literature [13], though a considerable degree of latitude in these remain.

We solve Eq. (3) and Eq. (4)

$$A(t) = \frac{A_0}{\gamma_A}(1 - e^{-\gamma_A t}) + A_i e^{-\gamma_A t} \tag{5}$$

$$T(t) = \frac{T_0}{\gamma_T}(1 - e^{-\gamma_T t}) + T_i e^{-\gamma_T t} \tag{6}$$

where, $A_i = A(0)$ and $T_i = T(0)$. Substituting of $A(t)$ and $T(t)$ in Eq. (2):

$$\frac{dn}{dt} = rn(1 - \frac{n}{K}) + mn(1 - e^{-\gamma_A t}) + pne^{-\gamma_A t} - qn(1 - e^{-\gamma_T t}) - sne^{-\gamma_T t} \tag{7}$$

here, $m = \frac{\alpha A_0}{\gamma_A}, p = \alpha A_i, q = \frac{\beta T_0}{\gamma_T}$ and $s = \beta T_i$. There is no prior presence of iAs and tea in the mice. Normal tap water, given to the mice, is tested for iAs (using atomic absorption spectroscopy (AAS)). The used tap water was found to be free of the metalloid As. The presence of iAs at a very small level in the body cannot be ruled out, but that is negligible for the model and beyond experimental control. Values of iAs and tea at $t = 0$ i.e., A_i, T_i is set to 0. This clearly implies $p, s = 0$. In the present problem, $\gamma_A = 0.04\ \text{day}^{-1}$ and $\gamma_T = 4\ \text{day}^{-1}$. We reiterate that these values are mere approximations, though within reasonable ranges. The depend on a host of factors, primarily the organ being considered, the method of administration and the measurement protocol. The values we use are in line with Hughes et al. [13] Numerically solving and fitting Eq. (7) to the given datasets, the values of unknown coefficients we obtain are: $r = 0.00524$, $K = 0.14706$, $m = 0.01281$ for the first dataset and $r = 0.01380$, $K = 0.21644$, $m = 0.00792$, $q = 0.00041$ for the second. For the first dataset, the effect of black tea is not included obviously and q is irrelevant for the first dataset.

The curves fitted to the given datasets are shown in Fig. 2: red and green dots are experimental data. It is clear that the fitting is very good for both the curves. Although iAs has a much longer half-life in comparison to black tea, the competition between the damage by iAs and mitigation by tea is clearly visible from both the data and the model. The saturation value and time to reach saturation for the growth with tea and iAs (lower curve) is considerably lower than the upper curve with only iAs. It is quite redeeming that from the experiment and the model, the effect of tea is found to be appreciable.

That the curves for iAs alone and iAs and tea in tandem could both be fitted with similar models, gives confidence on the model considered above. This could then be used for further predictions. A prediction from this is that the damage appears to saturate in both cases, though earlier for the case with tea. This kind of saturation implies that the damage could be limited by an external mitigant like black tea. As mentioned before, we have not added the effects of immunogenicity above, which will indeed abet early saturation. In the present paper we took the actual data for modelling, which makes it much more relevant. However, we underline the remit of data-fitting by mathematical equations once again: such exercise must be carried out with caution. With the absence of cellular level data on the concentration of iAs and black tea, add to it the inherent uncertainty and fluctuation in their values in situ, the predictions from the model are only indicative at this stage. As we show below, the immune-cell response dramatically alters the model, bringing it a lot closer to reality [8].

4. Growth model with immune cells

Choose $I(t)$ to denote immune cell count at any instance of time t with a constant influx of I_0 and if the death rate of immune cells is γ_I, the overall dynamics may then be represented by the following four equations:

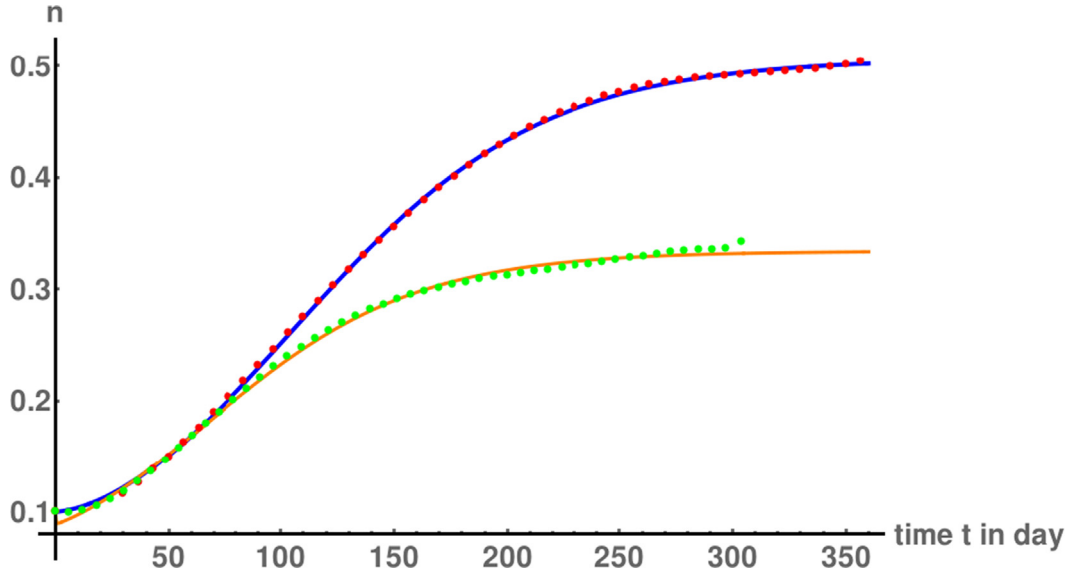

Fig. 2 Fitting of curves to the given data. Red and green dots represent experimental data and the blue and orange lines represent the fitted curves.

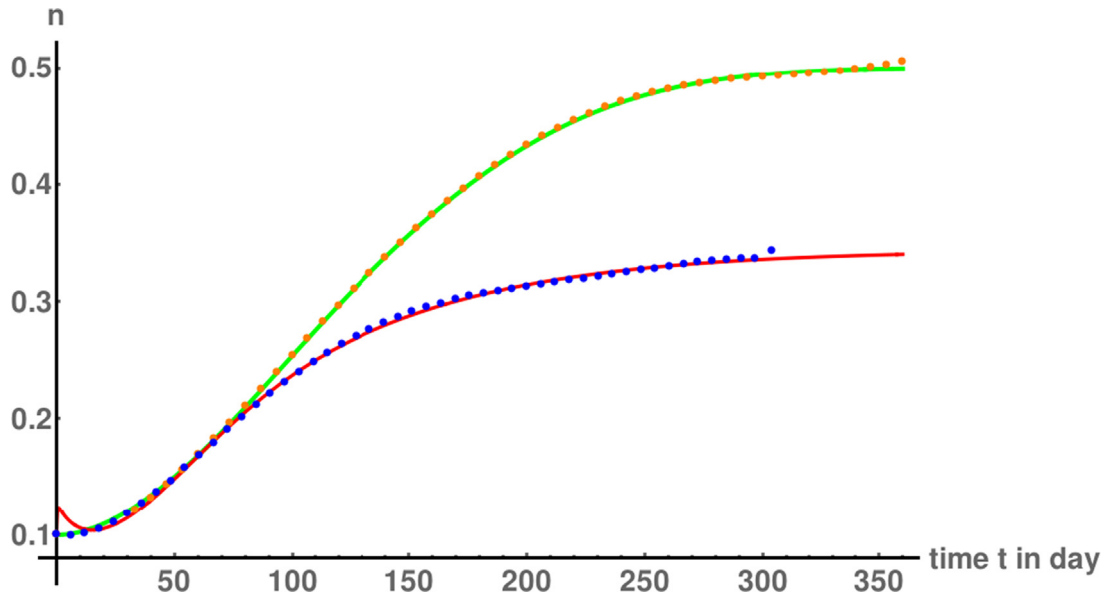

Fig. 3 Fitting of the datasets as discussed in text. The dotted orange and blue curves represent experimental data and the green and red solid lines are our fitting.

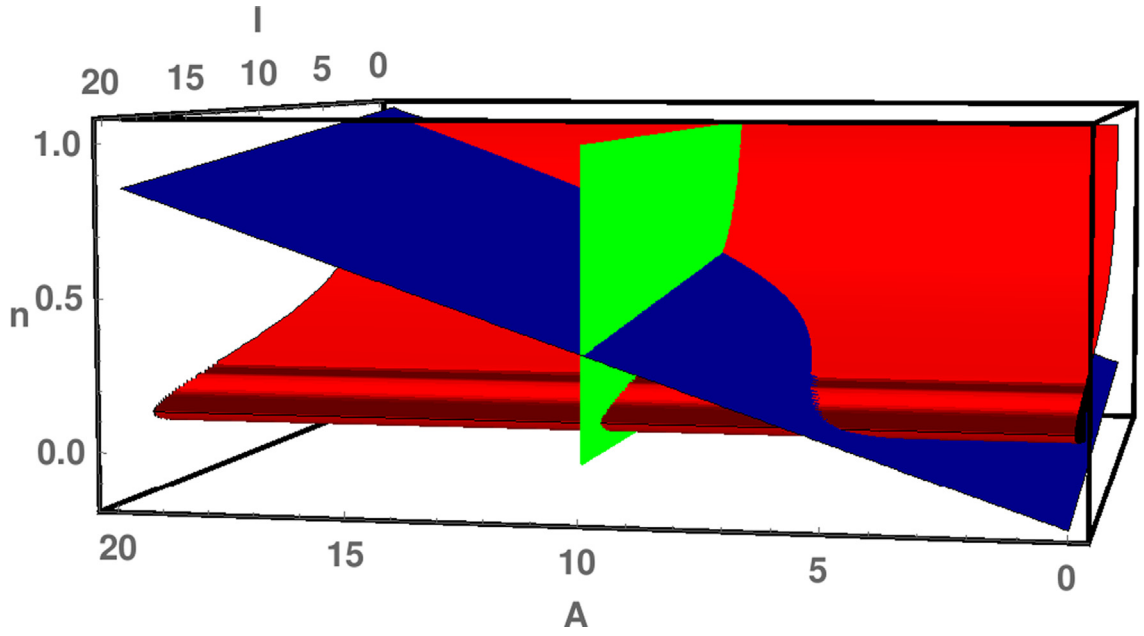

Fig. 4 Three null-surfaces from Eqs. (13)–(15) are shown using the coefficients from fitting. Here $A_0 = 0.4$. The points of equilibrium (n^*, A^*, I^*) would be at the intersections of the three surfaces.

$$\frac{dn}{dt} = rn(1 - \frac{n}{K}) + \alpha An - \beta nT - \epsilon nI \tag{8}$$

$$\frac{dA}{dt} = A_0 - \gamma_A A \tag{9}$$

$$\frac{dT}{dt} = T_0 - \gamma_T T \tag{10}$$

$$\frac{dI}{dt} = I_0 + \frac{\rho In}{\alpha_1 + n} - c_1 In - \gamma_I I \tag{11}$$

The rates of decay of iAs and black tea (γ_A and γ_T) were already given in the section above. It is not difficulty to check the existence and uniqueness of solution of the above model for a given initial condition (n_0, A_0, T_0, I_0). Since the right hand side function is Lipschitz, one can apply Picard-Lindeloff theorem to ensure the existence and uniqueness of solution.

In the dynamics of immune cells, the second term above represents the usual kinetics dictated by Michaelis-Menten expression. A constant influx rate of the immune cells $I_0 = 0.3$ and the rate of decay of the immune cells $\gamma_I = 0.0208$ day^{-1} is considered [9,20]. Eqs. (9) and (10) are analytically solved

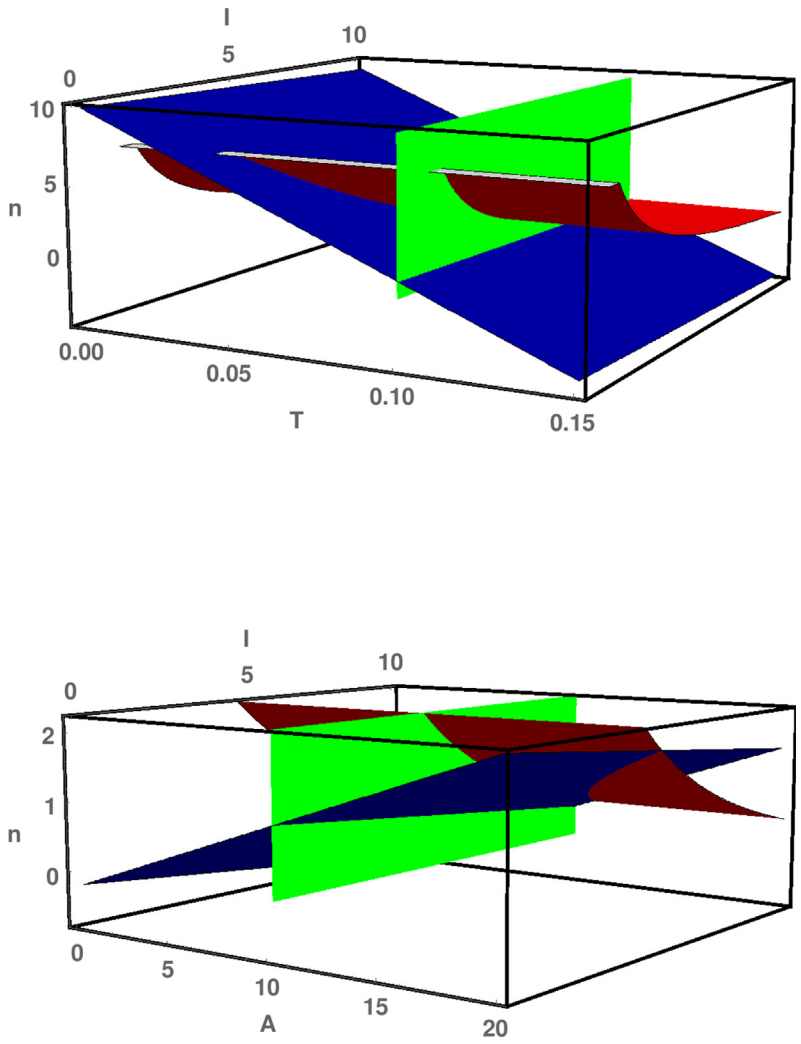

Fig. 5 Three null-surfaces from Eqs. (18)–(21) using the coefficients obtained by the fitting. We have taken $A_0 = 0.4$ and $T_0 = 0.4$ above. For plotting the upper one A is ket fixed at $A = A^* = 10$ and in the lower one, the null-surfaces are shown with T fixed at $T = T^* = 0.1$. Equilibrium points (T^*, I^*, n^*) and (A^*, I^*, n^*) appear where these surfaces intersect.

and given in Eqs. (5) and 6. Substituting the expressions for $A(t)$ and $T(t)$ in Eq. (8) obtained analytically, one gets

$$\frac{dn}{dt} = rn(1 - \frac{n}{K}) + mn(1 - e^{-\gamma_A t}) + pne^{-\gamma_A t} - qn(1 - e^{-\gamma_T t}) - sne^{-\gamma_T t} - \epsilon nI \tag{12}$$

here, the unknown coefficients $m\ (= \frac{\alpha A_0}{\gamma_A})$, $p\ (= \alpha A_i)$, $q\ (= \frac{\beta T_0}{\gamma_T})$, $s\ (= \beta T_i)$, ϵ, ρ, α_1 and c_1 are going to be fitted from the data we have. Initially ($t = 0$), no iAs, tea and immune cells are present. This is reasonable to assume though pre-existing iAs and immune cells cannot be ruled out altogether. Even if they existed, the numbers are taken to be small and negligible. It implies $A_i, T_i = 0$ and therefore the corresponding coefficients $p, s = 0$.

We solve Eqs. (11) and (12) numerically and on fitting with experimental data, the values of the unknown coefficients we obtain are: $r = 0.00173$, $K = 0.03166$, $m = 0.02802$, $\epsilon = 0.00055$, $\rho = 0.95103$, $\alpha_1 = 1.30187$, $c_1 = 0.63433$ for the first set of data and $r = 0.60516$, $K = 8.97523$, $m = 0.08006$, $q = 0.61760$, $\epsilon = 0.00379$, $\rho = 0.02733$, $\alpha_1 = 2.15877$, $c_1 = 0.02718$ for the second. The coefficients for the first set are calculated without considering the effects coming from tea. The curves that fit are shown in Fig. 3 along with the experimental data points, shown by the orange and blue color dots.

4.1. Equilibria

4.1.1. Tea-free equilibria

To study the equilibria, the case without tea is considered first. The steady state solutions are obtained as:

$$\dot{n} = 0$$

$$\dot{A} = 0$$

$$\dot{I} = 0$$

Note that $n = 0$ solutions are not experimentally relevant. So we only look for the non-zero n solution only. The Eqs. above

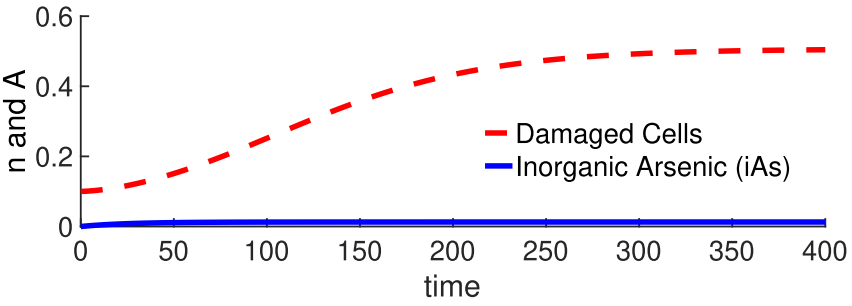

Fig. 6 The solution curves corresponding to the model system (2) and (3).

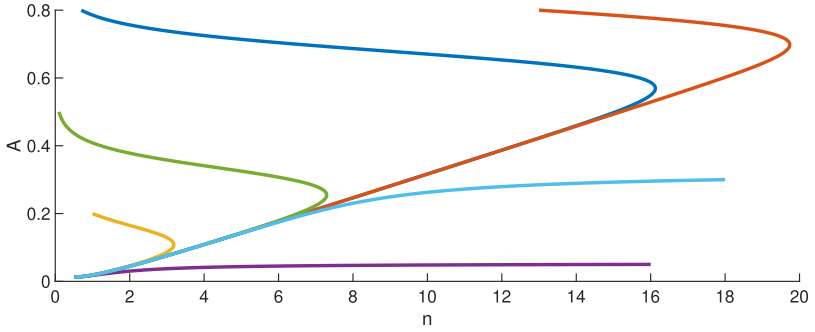

Fig. 7 Phase-portrait of the model system (2) and (3). The solution trajectories converge to the interior steady state (0.5034, 0.01281), emerging from different initial points.

give three null surfaces, and their intersection give the desired equilibrium point (n^*, A^*, I^*). We derive the non-trivial solutions:

$$n^* = K\left(1 + \frac{\alpha A^*}{r} - \frac{\epsilon I^*}{r}\right) \tag{13}$$

$$A^* = \frac{A_0}{\gamma_A} \tag{14}$$

$$I^* = \frac{I_0(\alpha_1 + n^*)}{c_1\alpha_1 n^* + c_1 n^{*2} + \gamma_I\alpha_1 + \gamma_I n^* - \rho n^*} \tag{15}$$

As mentioned above, the trivial equilibrium $n^* = 0$ is studied by other authors [8], it does not correspond to a experimentally relevant outcome. We do not consider the trivial point thus. We plot the three null-surfaces given by Eqs. (13)–(15) in Fig. 4, using the values of the coefficients obtained earlier from the fit. Numerically solving Eqs. (13) and (15) and using the values of the coefficients, the equilibrium is found to occur at $(A^*, I^*, n^*) = (10, 4.010730, 0.502892)$. Here we the constant influx of iAs was set at $A_0 = 0.4$. Once the non-trivial equilibria are obtained, we go ahead and work out their linear stability. The positivity of equilibria need to be maintained and therefore we need $r + \alpha A^* > \epsilon I^*$ and $\rho < c_1\alpha_1 + \gamma_I$. From an observation of the roots, we obtain the other condition $c_1 n^{*2} + (c_1\alpha_1 + \gamma_I - \rho)n^* + \gamma_I\alpha_1 = c_1 n^{*2} + bn^* + \gamma_I\alpha_1 = (n^* - a_1)(n^* - a_2)$,. Here $a_{1,2} = \frac{1}{2c_1}(-b \pm \sqrt{b^2 - 4c_1\gamma_I\alpha_1})$.

4.1.2. Analysis of stability

A Jacobian matrix can be constructed:

$$J = \begin{pmatrix} \alpha A^* - \epsilon I^* + r - \frac{2r}{K}n^* & \alpha n^* & -\epsilon n^* \\ 0 & -\gamma_A & 0 \\ \frac{\rho I^*}{\alpha_1 + n^*} - \frac{\rho I^* n^*}{(\alpha_1 + n^*)^2} - c_1 I^* & 0 & \frac{\rho n^*}{\alpha_1 + n^*} - c_1 n^* - \gamma_I \end{pmatrix}$$
$$= \begin{pmatrix} L^* & \alpha n^* & -\epsilon n^* \\ 0 & -\gamma_A & 0 \\ M^* & 0 & P^* \end{pmatrix}$$

where $L^* = \alpha A^* - \epsilon I^* + r - \frac{2r}{K}n^*, M^* = \frac{\rho I^*}{\alpha_1 + n^*} - \frac{\rho I^* n^*}{(\alpha_1 + n^*)^2} - c_1 I^*$ and $P^* = \frac{\rho n^*}{\alpha_1 + n^*} - c_1 n^* - \gamma_I$

The corresponding eigenvalues of the Jacobian matrix are:

$$\lambda_1 = -\gamma_A < 0 \tag{16}$$

$$\lambda_\pm = \frac{1}{2}\left[(L^* + P^*) \pm \sqrt{(L^* - P^*)^2 - 4\epsilon n^* M^*}\right] \tag{17}$$

The eigenvalues must have their real parts negative for stability. So, we find the region corresponding to the negative eigenvalues in the $n - I - A$ axes. The values obtained for n^*, A^* and I^* are shoved back in Eq. (17) to get $\lambda_\pm < 0$. As the real part of λ_1 is negative, it implies stable equilibrium.

4.1.3. With-tea equilibrium

The same procedure leads to a solution of the equations:

$$\dot{n} = 0$$

$$\dot{A} = 0$$

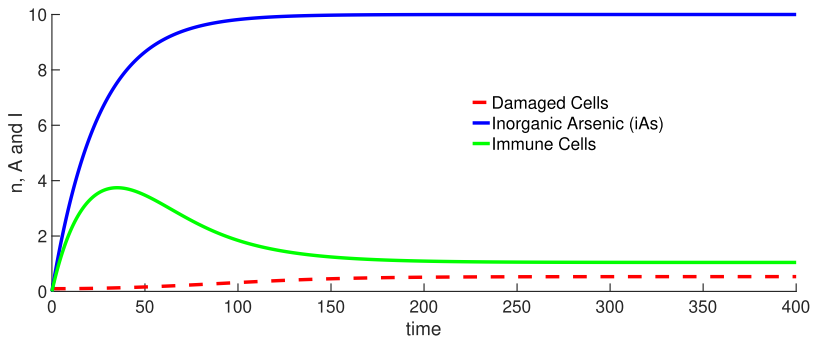

Fig. 8 The solution curve for model system (8)–(11). The solution curve converges to its interior steady state (0.5338, 10, 1.1046), having started from (0.1, 0, 0).

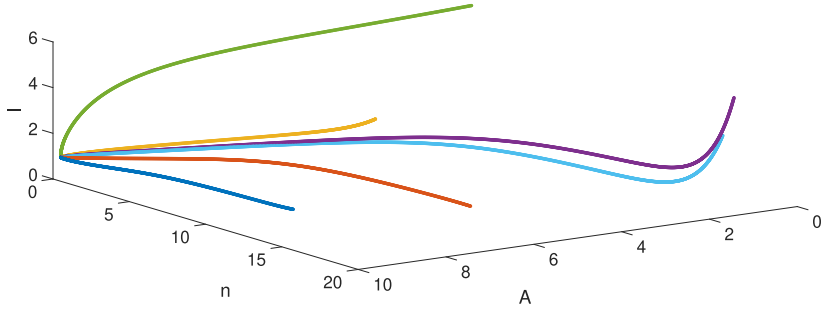

Fig. 9 The phase-portrait for model system (8)–(11). The Solution trajectories converge to interior steady state (0.5338, 10, 1.1046) having started from separate points.

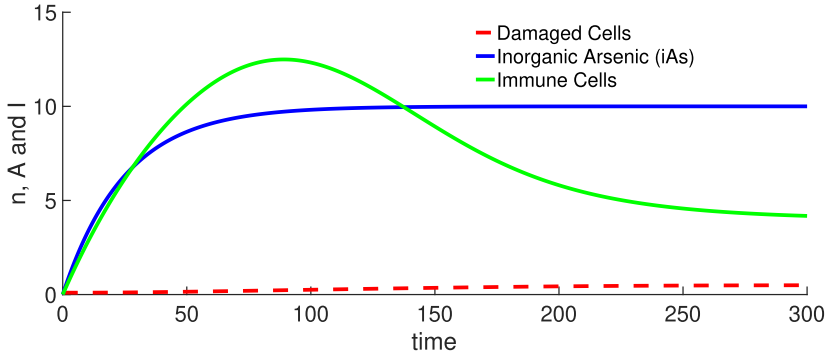

Fig. 10 The solution curve for model system (8)–(11) without tea. the curve converges to its interior steady state $(n^*, A^*, I^*) = (0.502892, 4.010730, 10)$ initiating from (0.1, 0, 0). The parametric values are the same as for the first experimental set of data.

$$\dot{T} = 0$$

$$\dot{I} = 0$$

Finally the non-zero solutions we get:

$$n^* = K\left(1 + \frac{\alpha A^*}{r} - \frac{\beta T^*}{r} - \frac{\epsilon I^*}{r}\right) \tag{18}$$

$$A^* = \frac{A_0}{\gamma_A} \tag{19}$$

$$T^* = \frac{T_0}{\gamma_T} \tag{20}$$

$$I^* = \frac{I_0(\alpha_1 + n^*)}{c_1\alpha_1 n^* + c_1 n^{*2} + \gamma_I\alpha_1 + \gamma_I n^* - \rho n^*} \tag{21}$$

In order to ensure the positivity of equilibria, $r + \alpha A^* > \beta T^* + \epsilon I^*$ and therefore $\rho < c_1\alpha_1 + \gamma_I$. The equilibrium points (T^*, I^*, n^*) and (A^*, I^*, n^*) can be read off from the figures in Fig. 5. As before, they appear at the intersections of these surfaces.

4.1.4. Stability analysis

The 4×4 Jacobian Matrix is now

$$J = \begin{pmatrix} L^* & \alpha n^* & -\beta n^* & -\epsilon n^* \\ 0 & -\gamma_A & 0 & 0 \\ 0 & 0 & -\gamma_T & 0 \\ M^* & 0 & 0 & P^* \end{pmatrix}$$

where

$L^* = \alpha A^* - \beta T^* - \epsilon I^* + r - \frac{2r}{K} n^*$, $M^* = \frac{\rho I^*}{\alpha_1 + n^*} - \frac{\rho I^* n^*}{(\alpha_1 + n^*)^2} - c_1 I^*$

and $P^* = \frac{\rho n^*}{\alpha_1 + n^*} - c_1 n^* - \gamma_I$. Note that the both the eigenvalues of the Jacobian above, $\lambda_1 = -\gamma_A$ and $\lambda_2 = -\gamma_T$ are negative. The two other eigenvalues:

$$\lambda_\pm = \frac{1}{2}\left[(L^* + P^*) \pm \sqrt{(L^* - P^*)^2 - 4\epsilon n^* M^*}\right] \tag{22}$$

We look for the regions where the real part of $\lambda_\pm < 0$. Fig. 5, shows the three null-surfaces given by Eqs. (18)–(21), where we used the coefficients from the fitting again; the upper one is when A is fixed at $A^* = 10$. For the lower, the null-surfaces are plotted with T kept fixed at $T^* = 0.1$. As before, the points of equilibrium (T^*, I^*, n^*) and (A^*, I^*, n^*) come from the intersections of these surfaces. We find that equilibrium appears at the point $(A^*, T^*, I^*, n^*) = (10,\ 0.1,\ 11.48990,\ 0.35624)$, where the constant rates of influx of iAs and tea have been fixed at $A_0, T_0 = 0.4$. As we substitute the values for n^*, A^*, T^* and I^* in Eq. (22), it is observed that the real part of $\lambda_\pm < 0$. Note that the real parts of the other two eigenvalues are negative already. So this implies that the coefficients obtained from the fit do indeed give us stable equilibrium.

4.2. Model including delay

Indeed, immune response is usually a delayed response in any living organism and therefore it is natural that a delay in $I(t)$ in the functional response term needs to be included for the sake of connection to reality. And then the overall dynamics of the system should be represented by the set of equations:

$$\begin{aligned} \tfrac{dn(t)}{dt} &= rn(t)(1 - \tfrac{n(t)}{K}) + \alpha A(t)n(t) - \beta n(t)T(t) - \epsilon n(t)I(t) \\ \tfrac{dA(t)}{dt} &= A_0 - \gamma_A A(t) \\ \tfrac{dT(t)}{dt} &= T_0 - \gamma_T T(t) \\ \tfrac{dI(t)}{dt} &= I_0 + \tfrac{\rho I(t-\tau)n(t)}{\alpha_1 + n(t)} - c_1 I(t)n(t) - \gamma_I I(t), \end{aligned} \tag{23}$$

The history conditions are: $n(0) = n_0, A(0) = A_0, T(0) = T_0, I(t) = \phi(t)$ for $t \in [-\tau, 0]$.

4.2.1. Stability without tea

The stability of (non-trivial) equilibrium solutions are revealed in the following. The set of equilibria are the same as with Eqs. (8)–(11). We analyze first the tea-free situation.

As before, we the Jacobian matrix is constructed:

$$\Delta(\lambda, \tau) = det \begin{pmatrix} (\alpha A^* - \epsilon I^* + r - \frac{2r}{K} n^*) - \lambda & \alpha n^* & -\epsilon n^* \\ 0 & -\gamma_A - \lambda & 0 \\ \frac{\rho I^*}{\alpha_1 + n^*} - \frac{\rho I^* n^*}{(\alpha_1 + n^*)^2} - c_1 I^* & 0 & (\frac{\rho n^* e^{-\lambda\tau}}{\alpha_1 + n^*} - c_1 n^* - \gamma_I) - \lambda \end{pmatrix} = det \begin{pmatrix} L^* - \lambda & \alpha n^* & -\epsilon n^* \\ 0 & -\gamma_A - \lambda & 0 \\ M^* & 0 & P_1^* + P_2^* e^{-\lambda\tau} - \lambda \end{pmatrix}$$

In the above equations $L^* = \alpha A^* - \epsilon I^* + r - \frac{2r}{K} n^*, M^* = \frac{\rho I^*}{\alpha_1 + n^*} - \frac{\rho I^* n^*}{(\alpha_1 + n^*)^2} - c_1 I^*, P_1^* = -c_1 n^* - \gamma_I$ and $P_2^* = \frac{\rho n^*}{\alpha_1 + n^*}$. Use the stability criteria (see Theorem 3.7.1 in Gopalaswamy [11]) for a nonlinear delay equation:

Theorem 1. *The necessary and sufficient conditions for any equilibrium to be asymptotically stable, for all $\tau \geqslant 0$, are: (1) The root of $\Delta(\lambda, 0) = 0$ must have negative real parts.*

(2) $\Delta(i\mu, \tau) \neq 0$, for all real μ and all $\tau \geqslant 0$.

An eigenvalue here is trivially $-\gamma_A$ and others are obtained from the root of

$$(L^* - \lambda)(P_1^* + P_2^* e^{-\lambda\tau} - \lambda) + \epsilon n^* M^* = 0.$$

Simplifying, we get

$$\lambda^2 + (-L^* - P_1^* - P_2^* e^{-\lambda\tau})\lambda + L^*(P_1^* + P_2^* e^{-\lambda\tau}) + \epsilon n^* M^* = 0.$$

The condition for non-delayed case was already found out. For the other condition, we substitute $\lambda = i\mu$ above,

$$-\mu^2 + (-L^* - P_1^* - P_2^* e^{-i\mu\tau})i\mu + L^*(P_1^* + P_2^* e^{-i\mu\tau}) + \epsilon n^* M^*$$

On separating real and imaginary parts,

$$\begin{aligned} -\mu^2 - P_2^* \sin(\mu\tau)\mu + P_2^* \cos(\mu\tau) + \epsilon n^* M^* = 0 \\ -L^* - P_2^* \cos(\mu\tau)\mu - P_2^* \sin(\mu\tau) = 0. \end{aligned} \tag{24}$$

Then, squaring and adding,

$$(\epsilon n^* M^* - \mu^2)^2 + L^{*2} = P_2^{*2}\mu^2 + P_2^{*2},$$

which further implies

$$\mu^4 - ((P_2^*)^2 + 2\epsilon n^* M^*)\mu^2 + \epsilon^2 n^{*2} M^{*2} + L^{*2} - P_2^{*2} = 0.$$

Now the roots are:

$$\mu_\pm^2 = \frac{1}{2}\left[((P_2^*)^2 + 2\epsilon n^* M^*) \pm \sqrt{((P_2^*)^2 + 2\epsilon n^* M^*)^2 - 4(\epsilon^2 n^{*2} M^{*2} + L^{*2} - P_2^{*2})}\right]$$

Condition (2) of the theorem is violated, implying that there exists a μ such that the above relation holds. It holds when $\epsilon^2 n^{*2} M^{*2} + L^{*2} > P_2^{*2}$; the equilibrium is stable if in addition to the condition for non-delay case (Section 4.1.2), $\epsilon^2 n^{*2} M^{*2} + L^{*2} < P_2^{*2}$ is also satisfied.

Remark 1. With-tea – the stability of equilibrium: Since the equation in I now does not depend on T, the same condition obtains for the stability: $\epsilon^2 n^{*2} M^{*2} + L^{*2} < P_2^{*2}$ in addition to the one in the subSection (4.1.4).

5. Numerical simulations

Numerical examples and their simulations are presented here to validate the analytical and stability results of the previous sections. We show numerical experiments for all the cases with different sets of parameters.

5.1. Model systems with no delay

We solve the model systems numerically without delay first. We then discuss both cases, i.e., with and without tea.

5.1.1. Without tea

Consider the parameter values given in Eq. (25). They denote the parametric values corresponding to the model systems (2) and (3) (i.e., system without tea as well as immune cells).

$$r = 0.00524, K = 0.14706, \alpha = 1, A_0 = 0.0005124, \gamma_A = 0.04, \tag{25}$$

Given the parametric values in (25), the model system (2) and (3) gives an interior equilibrium solution in $\mathbb{R}^2_+$, namely $(n^*, A^*) = (0.5034, 0.01281)$. The solution curves approach the steady state starting from the initial condition (0.1, 0) (the solution curves shown in Fig. 6 are referred here as also the phase plain in Fig. 7).

$$r = 0.00173, K = 0.03166, \alpha = 0.0002802, A_0 = 0.4, \gamma_A = 0.04, I_0 = 0.3,$$
$$\alpha_1 = 1.30187, c_1 = 0.63433, \gamma_1 = 0.0208, \rho = 0.25, \epsilon = 0.00055 \tag{26}$$

In the case of the parametric values in (26), the model system (8), (9) and (11) (non-delayed model system, no tea), admits of a steady state solution $(n^*, A^*, I^*) = (0.5338, 10, 1.1046)$. The solution curves stabilizing to their steady state, shown in Fig. 8. Corresponding phase-portrait of the model system (8), (9) and (11) is described in Fig. 9.

Here, for the parametric values in (26), we have $r + \alpha A^* = 0.03148 > \epsilon I^* = 0.00061, \rho = 0.25 < c_1\alpha_1 + \gamma_I = 0.84661$, $L^* = -0.02747 < 0, P^* = -0.208974 < 0$ and hence $L^* + P^* < 0$ and also $L^*P^* - \epsilon M^* n^* = 0.00591 > 0$. The positivity and local stability conditions for the steady state solution (n^*, A^*, I^*) of Section 4 also agree.

In the following, we solve the model system (8), (9) and (11) using the parametric values of the experimental data set (the first one, in Section 4). These values were calculated without the effect of black tea. They are same as the ones given in (26), except $\rho = 0.95103$. The solution curves for system (8), (9) and 11 with parametric values from first experimental data set show that all the populations stabilizes to its steady state solution $(n^*, A^*, I^*) = (10, 4.010730, 0.502892)$ (refer the Fig. 10).

We may therefore get stable solutions the regions of stability.

5.1.2. Model systems, with-tea

The graphical interpretations for the solution trajectories of the model system (2)–(4) in the presence of tea cells are discussed here. Taking parametric values from (27) for the model system (2)–(4) (non-delayed model system with tea and no immune cells), we write:

$$r = 0.01380, K = 0.21644, \alpha = 1, \beta = 1, A_0 = 0.0003168, \gamma_A = 0.04,$$
$$\gamma_T = 4, T_0 = 0.00164 \tag{27}$$

Consider the parametric values in (27), the model system (2)–(4) has a steady state solution $(n^*, A^*, T^*) = (0.3338, 0.00792, 0.00041)$ and the solution curves stabilize to its steady state (shown in Fig. 11). The phase portrait of the model system (2)–(4) has been shown in Fig. 12.

$$r = 0.60516, \quad K = 8.97523, \quad \alpha = 0.008006, \quad A_0 = 0.4, \quad \gamma_A = 0.04, \quad \gamma_T = 4,$$
$$T_0 = 0.4, \quad \rho = 0.0073, \quad \alpha_1 = 2.15877, \quad c_1 = 0.02718, \quad \gamma_1 = 0.0208, \quad I_0 = 0.3 \tag{28}$$

For the values of parameters given in (28), the model system (8)–(11) (non-delayed model system with tea and immune cells), admits of a steady state solution $(n^*, A^*, T^*, I^*) = (0.4838, 10, 0.1, 9.21)$ and the solution curves converge to the steady state solution (refer Fig. 13). For the parametric values in (28), $r + \alpha A^* = 0.68522 > \beta T^* + \epsilon I^* = 0.6525$, $\rho = 0.0073 < c_1\alpha_1 + \gamma_I = 0.07948, L^* = -0.00840 < 0, P^* = -0.22946 < 0$ and hence $L^* + P^* < 0$ and also $L^*P^* - \epsilon M^* n^* = 0.00069 > 0$. The conditions for the positivity and local

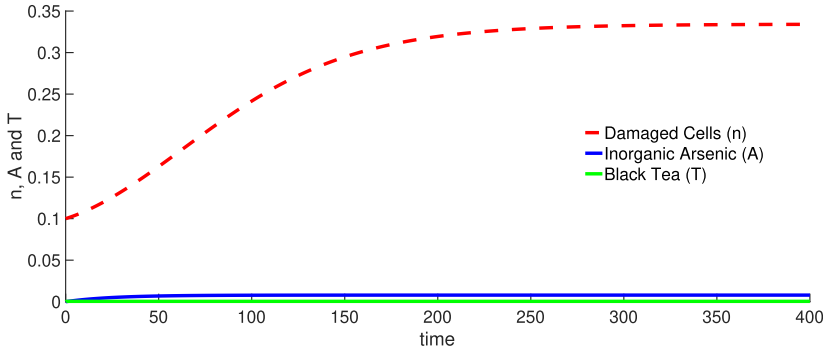

Fig. 11 The solution curve for model system (2)–(4). Solution curve converges to its interior steady state (0.3338, 0.0.00792, 0.00041) initiating from (0.1, 0, 0).

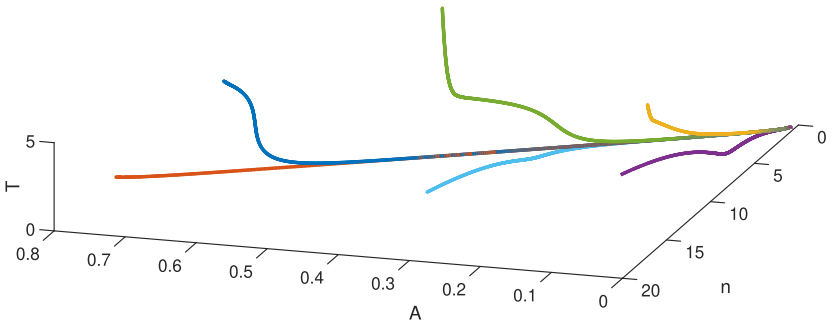

Fig. 12 Phase portrait for model system (2)–(4). Solution trajectories converges to its interior steady state (0.3338, 0.00792, 0.00041) starting from different initial points.

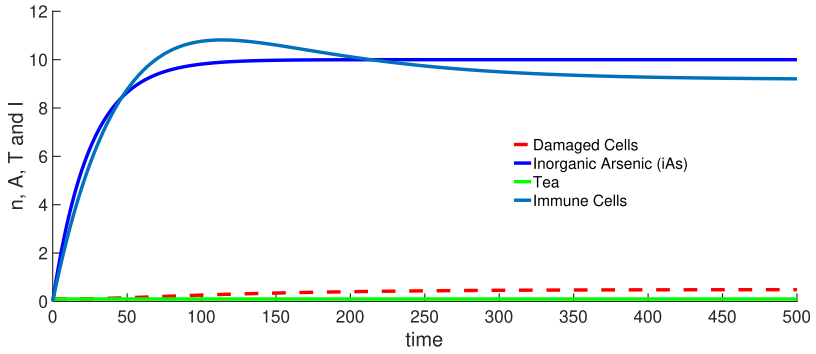

Fig. 13 Solution curve for model system (8)–(11). Solution curve converges to its interior steady state (0.4838, 10, 0.1, 9.21) initiating from (0.1, 0, 0, 0).

stability of steady state solution (0.4838,10,0.1,9.21) are therefore satisfied.

Now we solve the model system (8)–(11) for the parametric values obtained via second experimental data set (see Section 4). These parametric values are calculated with the effect of black tea and are same as parametric given in (28) except $\rho = 0.02733$. The solution curves for system (8)–(11) with parametric values from second experimental data set show that all the populations stabilizes to its steady state solution $(n^*, A^*, T^*, I^*) = (0.3564, 10, 0.1, 11.48990)$ (refer the Fig. 14).

5.2. Model systems with delay

Now here we discuss solution curves for the model systems with delay in immune response for both the cases with tea and without tea.

5.2.1. Model systems without tea

We consider same set of parametric values taken as in (26) for immune system without tea (i.e., model system with first, second and fourth equation of (23)). For the parametric values in (26), the steady state solution of delayed model system

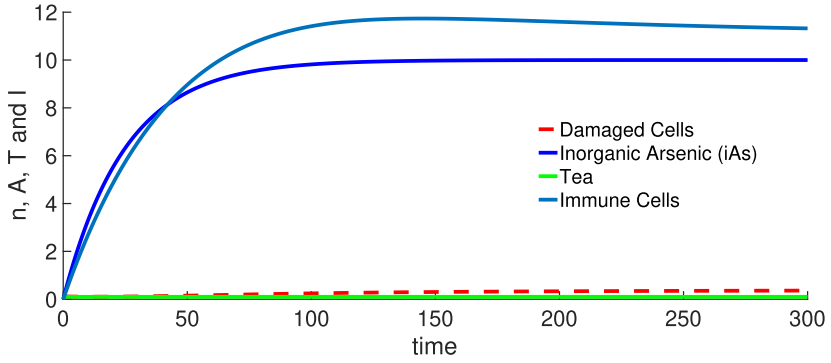

Fig. 14 Solution curve for model system (8)–(11) with black tea. Solution curve converges to its interior steady state $(n^*, A^*, T^*, I^*) = (0.3564, 10, 0.1, 11.48990)$ initiating from (0.1, 0, 0, 0). Parametric values are same as obtained by second experimental data set.

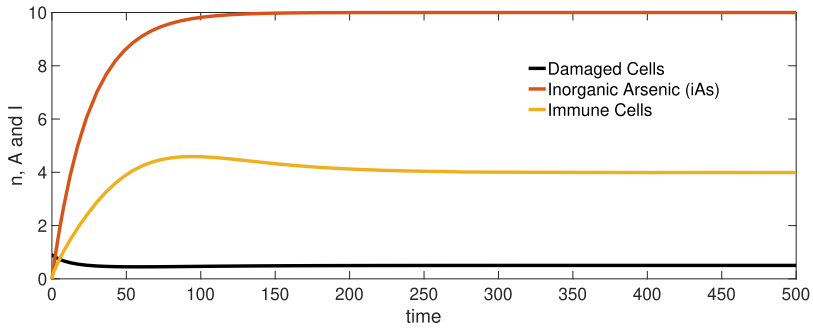

Fig. 15 Solution curve for the delayed model system (23) without tea. Solution curve converges to its interior steady state (0.5338, 10, 1.1046). Here $\tau = 2$.

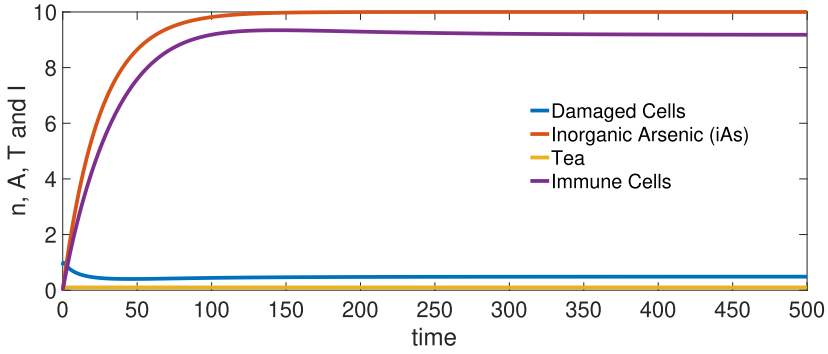

Fig. 16 Solution curve for the delayed model system (23) with tea. Solution curve converges to its interior steady state (0.4838, 10, 0.1, 9.21). Here $\tau = 2$.

(23) without tea is same as that of associated non-delayed system (8), (9) and (11). Here we have take the delay parameter $\tau = 2$. The positivity condition is same as in case of model system (8), (9) and (11), which we have already discussed. The stability condition is also well satisfied because $\epsilon^2 n^{*2} M^{*2} + P^{*2} = 0.00075 < M_2^{*2} = 0.022631$ (the reader may refer the Theorem 1). The solution curves are illustrated in the Fig. 15, which clearly converge to steady state equilibria.

5.2.2. Model systems with tea

Same set of parametric values, as in (28), are taken now for immune system with tea. We numerically solve the model system (23) adding delay and tea. The same set of parametric values are taken as in (28), considered for the corresponding non-delayed model (8)–(11). For the parameters in (28), the steady state solution of delayed model system (23) turns out to be the same as that of the associated non-delayed system (8)–(11). The delay parameter is taken to be $\tau = 2$. The positivity condition is the same as model system (8)–(11). As worked out in case of delayed model system in the absence of tea, one can easily show that $\epsilon^2 n^{*2} M^{*2} + L^{*2} < P_2^{*2}$(refer to the Remark 1). The corresponding solution curves are illustrated in the Fig. 16, and they converge to steady state equilibria.

Table 1 shows how the co-ordinates of the interior steady state changes if we change the constant rate of administration of tea (T_0) externally. We observe that initially the steady state value of damaged cell decreases slowly and after a certain value of T_0, it start decreasing more faster as we increase the value of T_0, while the just opposite happens for the steady state density of immune cells. Actually, due to faster increase of immune cell, the faster decrease of damaged cell occur.

Table 1 Interior equilibrium with respect to the constant rate of administration of tea (T_0) externally.

T_0	n^*	I^*
0.05	8.952	1.162
0.1	7.799	1.321
0.2	5.48	1.824
0.3	3.127	2.957
0.7	2.368e-96 ≡ 0	14.42

6. Conclusion

An attempt has been made to model the data obtained from the *in vivo* studies, using Swiss albino mice. Mice are maintained under the influence of iAs for a long period, with iAs-loaded water as the only source of drinking water. Black tea infusion is administered on a regular basis to a subset of the mice. The data obtained on the cell-damage in these two groups of mice were then modelled by the standard dynamical equations. It is redeeming to note that even simple models could fit the data well and predict long-term behavior of the cell damage by iAs and its alleviation by black tea. Further studies using experimentally obtained fitting parameters would reveal more interesting underlying dynamics that are testable in real systems. The predictions thereof would be reliable and useful for the study of growth and limitation of tumors.

Financial disclosure

None reported.

Declaration of Competing Interest

The authors declare that they have no known competing financial interests or personal relationships that could have appeared to influence the work reported in this paper.

Acknowledgments

We would like to thank the reviewers for their comments and suggestions. UD would like to acknowledge the Ministry of Human Resource Development (MHRD), India for research fellowship.

References

[1] P.M. Altrock, L.L. Liu, F. Michor, The mathematics of cancer: integrating quantitative models, Nat. Rev. Cancer 15 (2015) 730.
[2] Ahmad T. Ali, Mostafa M.A. Khater, C. Park, Abdel-Haleem Abdel-Aty, Raghda A.M. Attia, D. Lu, Abundant numerical and analytical solutions of the generalized formula of Hirota-Satsuma coupled KdV system, Chaos, Solit. Fract. 131 (2020), 109473.
[3] M. Balasubramanyam, A.A. Koteswari, R.S. Kumar, S.F. Monickaraj, J.U. Maheswari, V. Mohan, Curcumin-induced inhibition of cellular reactive oxygen species generation: novel therapeutic implications, J. Biosci. 28 (6) (2003) 715–721.
[4] J. Biswas, S. Roy, S. Mukherjee, D. Sinha, M. Roy, Indian spice curcumin may be an effective strategy to combat the genotoxicity of arsenic in Swiss albino mice, Asian Pacific J. Cancer Prev. 11 (1) (2010) 239–246.
[5] F. Castiglione, B. Piccoli, Cancer immunotherapy, mathematical modeling and optimal control, J. Theoret. Biol. 247 (2007) 23732.
[6] A. dOnofrio, A general framework for modeling tumor-immune systemcompetition and immunotherapy: mathematicalanalysis and biomedical inferences, Physica D 208 (2005) 220–235.
[7] L.G. de Pillis, A.E. Radunskaya, A mathematical tumor model with immune resistance and drug therapy: an optimal control approach, J. Theoret. Med. 3 (2001) 79–100.
[8] L.G. de Pillis, A. Radunskaya, The dynamics of an optimally controlled tumor model: a case study, Math. Comput. Modell. 37 (2003) 1221–1244.
[9] L.G. de Pillis, W. Gu, K.R. Fister, T. Head, K. Maples, A. Murugan, T. Neal, K. Yoshida, Chemotherapy for tumors: an analysis of the dynamics and a study of quadratic and linear optimal controls, Math. Biosci. 209 (2007), 292315.
[10] B. Ghanbari, S. Kumar, R. Kumar, A study of behaviour for immune and tumor cells in immunogenetic tumour model with non-singular fractional derivative, Chaos Solit. Fract. 133 (2020), 109619.
[11] K. Gopalsamy, Stability and Oscillation in Delay Differential Equations of Population Dynamics, Kluwer Academic, Dordrecht, 1992.
[12] I. Herath, M. Vithanage, J. Bundschuh, J.P. Maity, P. Bhattacharya, Natural arsenic in global groundwaters: distribution and geochemical triggers for mobilization, Curr. Pollut. Rep. 2 (2016) 68–89.
[13] M.F. Hughes, E.M. Kenyon, B.C. Edwards, C.T. Mitchell, L. M.D. Razo, D.J. Thomas, Accumulation and metabolism of arsenic in mice after repeated oral administration of arsenate, Toxicol. Appl. Pharmacol. 191 (3) (2003), 202210.
[14] V.D. Martínez, E.A. Vucic, D.D.B. Santos, L. Gil, W.L. Lam, Arsenic exposure and the induction of human cancers, J. Toxicol. 2011 (2011) 431287.
[15] D. Kirschner, J.C. Panetta, Modeling immunotherapy of the tumor-immune interaction, J. Math. Biol. 37 (1998) 235–252.
[16] I. Khairul, Q.Q. Wang, Y.H. Jiang, C. Wang, H. Naranmandura, Metabolism, toxicity and anticancer activities of arsenic compounds, Oncotarget 8 (14) (2017) 23905–23926.
[17] Mostafa M.A. Khater, C. Park, Abdel-Haleem Abdel-Aty, Raghda A.M. Attia, D. Lu, On new computational and numerical solutions of the modified ZakharovKuznetsov equation arising in electrical engineering, Alexandria Eng. J. 59 (3) (2020) 1099–1105.
[18] S. Kumar, R. Kumar, J. Singh, K.S. Nisar, D. Kumar, An efficient numerical scheme for fractional model of HIV-1 infection of CD4+ T-Cells with the effect of antiviral drug therapy, Alexandria Eng. J., DOI.org/10.1016/j.aej.2019.12.046
[19] R. Kumar, S. Kumar, A new fractional modelling on susceptible-infected-recovered equations with constant vaccination rate, Nonlinear Eng. 3 (1) (2014) 11–19.
[20] V.A. Kuznetsov, I.A. Makalkin, M.A. Taylor, A.S. Perelson, Nonlinear dynamics of immunogenic tumors: parameter estimation and global bifurcation analysis, Bull. Math. Bio. 56 (2) (1994) 295–321.
[21] P. Liu, X. Liu, Dynamics of a tumor-immune model considering targeted chemotherapy, Chaos Solit. Fract. 98 (2017) 7–13.
[22] H. Ohkawa, N. Ohishi, K. Yagi, Assay for lipid peroxides in animal tissues by thiobarbituric acid reaction, Anal. Biochem. 95 (1979) 351–358.
[23] R.R. Ramos, L.L. Carrillo, A.D.R. Perez, A.D.V. Ruíz, M.E. Cebrian, Sodium arsenite induces ROS generation, DNA oxidative damage, HO-1 and c-Myc proteins, NF-κB activation and cell proliferation in human breast cancer MCF-7 cells, Mutat. Res. 674 (1–2) (2009) 109–115.
[24] D. Sinha, S. Roy, M. Roy, Antioxidant potential of tea reduces arsenite induced oxidative stress in Swiss albino mice, Food Chem. Toxicol. 48 (4) (2010) 1032–1039.
[25] D. Sinha, M. Roy, M. Siddiqi, R.K. Bhattacharya, Modulation of arsenic induced DNA damage by tea as assessed by single cell gel electrophoresis, Int. J. Cancer Prevent. 2 (2) (2005) 143–154.
[26] D. Sinha, S. Roy, M. Roy, Antioxidant potential of tea reduces arsenite induced oxidative stress in Swiss albino mice, Food Chem. Toxicol. 48 (2010) 1032–1039.
[27] D. Sinha, M. Roy, Antagonistic role of tea against sodium arsenite-induced oxidative DNA damage and inhibition of DNA repair in swiss albino mice, J. Environ. Pathol. Toxicol. Oncol. 30 (4) (2011) 1–11.
[28] N.P. Singh, M.T. McCoy, R.R. Tice, E.L. Schneider, A simple technique for quantification of low levels of DNA damage in individual cells, Exp Cell Res. 175 (1988) 184–191.
[29] A.S. Tsao, E.S. Kim, W.K. Hong, Chemoprevention of cancer, CA A Cancer J. Clin. 54 (2004) 150–180.